Fit-to-Flow (F2F) interconnects: Universal reversible adhesive-free microfluidic adaptors for lab-on-a-chip systems†

Arnold Chen and Tingrui Pan*

Received 7th September 2010, Accepted 29th October 2010
DOI: 10.1039/c0lc00384k

World-to-chip (macro-to-micro) interface continues to be one of the most complicated, ineffective, and unreliable components in the development of emerging lab-on-a-chip systems involving integrated microfluidic operations. A number of irreversible (*e.g.*, adhesive gluing) and reversible techniques (*e.g.*, press fitting) have attempted to provide dedicated fluidic passage from standard tubing to miniature on-chip devices, none of which completely addresses the above concerns. In this paper, we present standardized adhesive-free microfluidic adaptors, referred to as Fit-to-Flow (F2F) Interconnects, to achieve reliable hermetic seal, high-density tube packing, self-aligned plug-in, reworkable connectivity, straightforward scalability and expandability, and applicability to broad lab-on-a-chip platforms; analogous to the modular plug-and-play USB architecture employed in modern electronics. Specifically, two distinct physical packaging mechanisms are applied, with one utilizing induced tensile stress in elastomeric socket to establish reversible seal and the other using negative pressure to provide on demand vacuum shield, both of which can be adapted to a variety of experimental configurations. The non-leaking performance (up to 336 kPa) along with high tube-packing density (of 1 tube/mm^2) and accurate self-guided alignment (of 10 μm) have been characterized. In addition, a 3D microfluidic mixer and a 6-level chemical gradient generator paired with the corresponding F2F Interconnects have been devised to illustrate the applicability of the universal fluidic connections to classic lab-on-a-chip operations.

Introduction

Advancements in lab-on-a-chip technologies have introduced a wide range of innovative and inspiring approaches to investigate cell biology,[1–3] molecular chemistry,[4–6] and physical phenomena[7–11] at micro- and nanoscales. Benefits of integrating cumbersome laboratory functions into the microfluidic platform result from its capability to allow multiplexed operations (*e.g.*, pumping, mixing and switching) over minute quantities of reagents (from picolitres to millilitres) in a highly precise and ultra-efficient process.[12,13] Despite the remarkable progression of the rapidly expanding on-chip functionalities, the world-to-chip (macro-to-micro) interface still remains one of the most complicated, ineffective, and unreliable steps in the development of lab-on-a-chip devices.[14]

Over the past decades, numerous efforts made to address the microfluidic connectivity issues can be categorized into two different approaches: irreversible and reversible packaging. Irreversible connection techniques, including surface chemical modified bonding[15–18] and adhesive-based gluing,[18–21] have been employed to permanently link the individual micro-devices to the external fluidic conduits. Although this permanent bonding strategy results in excellent non-leaking performance, the interconnects are usually bulky and unalterable. Additionally, gluing techniques using epoxies, uncrosslinked polymers, or UV-curable materials put the on-chip devices at risk of tubing/channel clogging.[22,23] In comparison, a reversible fluidic connection is often preferred in biological investigations and chemical analyses since it eliminates potential chemical cross-contamination, enables direct optical inspection and allows inexpensive disposable units. Present reversible connection techniques, such as press fitting of micro-tubes[24,25] and exterior casing of fluidic connections,[26–28] are capable of engaging and separating the micro-to-macro interface without severely affecting device structural integrity. In particular, Sabourin *et al.* recently introduced re-usable interconnection blocks to form reversible, aligned intermediates joining PMMA microfluidic chips to needle assemblies.[29] However, most of the current irreversible and reversible microfluidic packaging techniques are microfabrication-incompatible and difficult to miniaturize and/or integrate, which becomes the major bottleneck for emerging large-scale integrated and multitasking microfluidic implementation.[30,31]

In this paper, we present two simple strategies to achieve standardized adhesive-free microfluidic interfaces with hermetic seal performance (up to 336 kPa), high-density 2D tube-packaging (1 tube/mm^2), self-aligned plug-in, reworkable connectivity (device reusability), straightforward scalability and expandability, and applicability to broad lab-on-a-chip platforms, referred to as Fit-to-Flow (F2F) Interconnects. Analogous to the concept of universal serial bus (USB) in computer peripherals, molded PDMS blocks integrated with parallel micro-tube inserts form the female socket while pluggable on-chip components with complementary shapes (*i.e.*, the male piece) can be easily slid into the opening to establish direct microfluidic passage under

Micro-Nano Innovations (MiNI) Laboratory, Department of Biomedical Engineering, University of California, Davis, USA. E-mail: tingrui@ucdavis.edu

† Electronic supplementary information (ESI) available: Spring-loaded syringe for manual vacuum. See DOI: 10.1039/c0lc00384k

a mechanical seal. In particular, the first approach applies the press-fit principle to the microfluidic connectors as press Fit-to-Flow (*press-F2F*), in which the tensile stress in the elastomeric socket induced by the difference between the plug-in thickness and the socket height forms a tight seal around the interfaces. In contrast, the second vacuum Fit-to-Flow (*vacuum-F2F*) connection utilizes a negative pressure surrounding the fluidic conduits, either by a facility vacuum line or by a manual vacuum setup, to provide a high-performance reversible packaging. Moreover, fabrication of F2F Interconnects comprises only of single-step molding of polydimethysiloxane (PDMS) and plasma-activated bonding, which is among the simplest constructions of microfluidic interfaces. Furthermore, the replica mold of the elastomeric adaptors and the multilayer construct of the pluggable microfluidic chips are fabricated by an out-of-cleanroom process reported previously – the *Direct Projection on Dry-film Photoresist* (DP^2).[32] In addition, self-aligned structures are included in the reversibly pluggable design and enables simple yet precise positioning of the miniature fluidic openings, which become an exceedingly important feature when a large array of fluidic connections are necessary (*e.g.*, in large-scale integrated microfluidics). In brief, the F2F Interconnects offer universal connections in an expandable multi-channel configuration that can drastically extend and integrate the power of potent microfluidic operations in a similar manner as the general modular USB architecture employed in modern electronics.[33] The presented F2F Interconnects make the microfluidic chip disposable while keeping a standard plug-and-play interface for repetitive use. Fig. 1 shows a 3D microfluidic mixer consisting of multilayer fluidic network made of dry-film photoresists being plugged into a *press-F2F* connector with three access ports (2 inlets and 1 outlet).

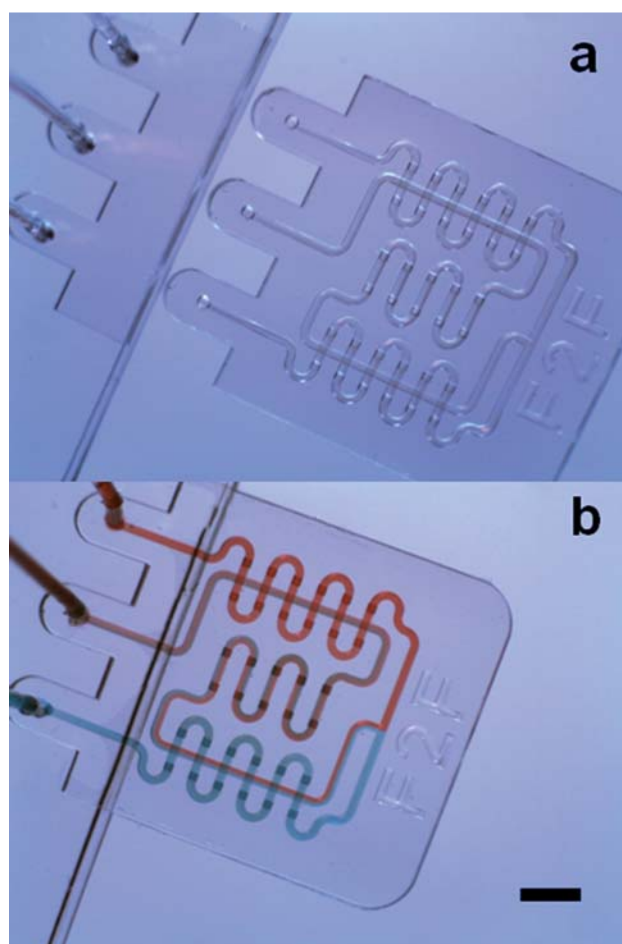

Fig. 1 A microscopic view of a 3D microfluidic mixer a) before and b) after plugging into a *press-F2F* connector (scale bar is 1mm).

Fit-to-Flow concepts

The proposed Fit-to-Flow schemes include two types of configurations sharing a similar interfacial architecture yet with distinct physical packaging mechanisms: one relying on induced elastomeric deformation to form press-fit seal (press Fit-to-Flow) and the other requiring a negative pressure to pull vacuum shield (vacuum Fit-to-Flow). As shown in Fig. 2, the elastomeric female socket seals the plugged-in microfluidic chip while circular PDMS through-holes allow Teflon micro-tube insertions.

In the *press Fit-to-Flow* (*press-F2F*) design, a fluidic seal forms when the tensile stress (σ_t) is induced by inserting a pluggable microfluidic chip with device thickness greater than the height of the PDMS socket. Primarily surrounding the socket borders, the magnitude of the stress depends linearly on the strain level (ε) and the elastic modulus (E) according to the stress–strain relationship of the elastic deformation.[34] The strain level can be calculated by the ratio of the height difference (Δh) between socket and microchip to the height of the socket opening (h), as illustrated in Fig. 2a. In addition, the material strength (*i.e.*, elastic modulus) of the microchip is expected to be greater than that of the socket construct, so mechanical deformation occurs primarily in the socket opening and does not compromise the on-chip fluidic performance. Eqn (1) shows the theoretical relationships among the leakage pressure (P_{fluid}), induced tensile stress and elastic deformation of the socket (*i.e.*, strain).

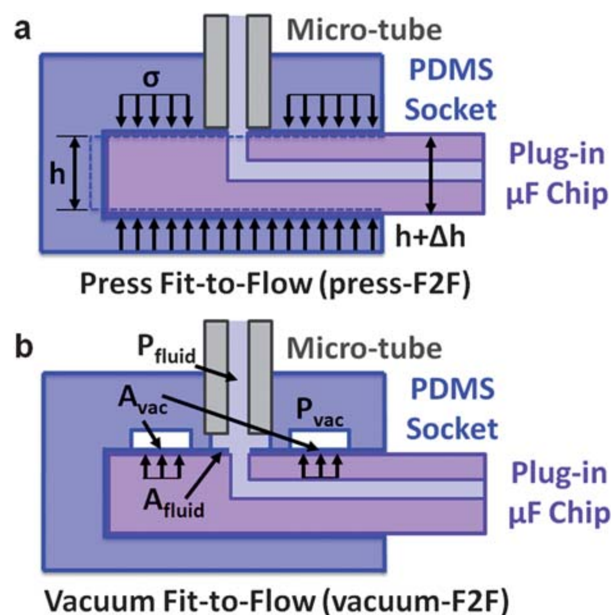

Fig. 2 Schematic illustration of the general principles of a) *press-F2F* using induced tension to seal and b) *vacuum-F2F* relying on vacuum shield formed by negative pressure.

 This journal is © The Royal Society of Chemistry 2010

$$P_{fluid} = \sigma_t = \varepsilon E = \frac{\Delta h}{h} E \quad (1)$$

Moreover, the complementary peg-like designs of the interconnect structures enable guided insertion and self alignment in a highly reliable manner. In brief, the *press-F2F* approach offers an easy-to-construct and universally applicable microfluidic connection with the plug-and-play feature.

The alternative implementation, the *vacuum Fit-to-Flow* (*vacuum-F2F*) device, utilizes negative pressure surrounding the fluidic conduits to provide on demand adhesive-free packaging for reversible connectivity. Unlike the *press-F2F* method, integrated o-ring designs surrounded by vacuum chambers, which are pneumatically connected to a dedicated vacuum port, are structurally placed around each access port in the PDMS layer as illustrated in Fig. 2b. In addition, elastomeric microposts are incorporated into the vacuum chambers to provide adequate mechanical support. Therefore, the overall reversible adhesion force from the vacuum-acting region balances the fluidic pressure exerted within the o-ring sealed structures. In other words, the leakage pressure can be determined by the vacuum-to-fluid area ratio (A_{vac}/A_{fluid}) and the vacuum pressure (P_{vac}) as expressed in eqn (2).

$$P_{fluid} = P_{vac} \frac{A_{vac}}{A_{fluid}} \quad (2)$$

Here, we have established the vacuum pressure by two easily accessible sources: a facility vacuum line generally available in chemical or biological labs, and a simple spring-loaded syringe, which will be described in detail in Results and Discussion. In comparison with the aforementioned press-fit design, the *vacuum-F2F* adaptor provides a reliable, reversible, controllable and expandable packaging strategy for diverse lab-on-a-chip applications, including large-scale integrated microfluidics.

Experimental

Fabrication of pluggable microchips

The pluggable microfluidic devices are prepared by the previously introduced DP^2 process in an out-of-cleanroom setting.[32] The fabrication process begins with the thermal lamination of dry-film resist (PerMX 3000, Dupont) onto a transient substrate and is soft baked at 115 °C for 5 min. The dry-film is then photo-exposed through a maskless projection setup (365 nm, 600 mJ cm^{-2}) to define the first layer of the device. Next, post-exposure bake is conducted at 95 °C for 2 min, followed by development with propylene glycol monomethyl ether acetate (PGMEA >99.5%, Sigma-Aldrich) in ultrasonic bath for 2 min. Subsequent structural layers of dry-film can be processed through the same repetitive steps of lamination, exposure, and development on top of the existing patterns to form enclosed microfluidic devices. Planar (2D) microfluidic networks are comprised of one structural layer along with top and bottom substrates while the 3D microfluidic chips are constructed with at least five dry-film layers to spatially steer microflow. Furthermore, integrated access ports (*e.g.*, inlets and outlets) travel transversally through multilayer constructs to the surface of the device. The plug-in side of the microfluidic chip is photo-defined with peg-like geometries complementary to the socket shape for guided insertion and self alignment (Fig. 3). The overall device height is controlled by adjusting the thickness of the top and/or bottom dry-film substrates, which can achieve various heights at spacings of every 5 μm. In addition to the dry-film polymer, the pluggable microchips in theory can be made from a wide range of materials including PDMS and other microfluidic constructs, *e.g.*, commonly used hybrid PDMS–glass devices.

Fabrication of elastomeric sockets

Fig. 3 shows the layer-by-layer assembly of the F2F elastomeric socket made of replica molded PDMS along with pluggable microchips. PDMS base and crosslink reagent mixed at 10 : 1 ratio (Sylgard 184, Dow Corning) is cured on a photopatterned dry-film mold with the identical profile as the plug-in edge of the microchips. Through-holes for micro-tube access (fluidic inlet/outlet and vacuum link) are manually punctured with a 21 gauge blunt needle at the designated locations corresponding to the access ports in the plug-in. Next, oxygen plasma treatment is performed to chemically activate the molded PDMS layer and a flat piece for seamless bonding and formation of the elastomeric socket. The newly created device has through-holes for allowing direct insertion of Teflon micro-tubes (of 150 μm ID and 360 μm OD, Upchurch Scientific) coupled to external fluidic conduits, while the socket enables reversible attachment and connection to microfluidic devices. Overall, the entire manufacturing process of F2F Interconnects is microfabrication-compatible.

Leakage tests

To perform the leakage test, the male pluggable components are fully inserted into the socket of the F2F interconnects. The desired mechanical seal is achieved in fluidic passage *via* tensile stress for *press-F2F* connectors, whereas *vacuum-F2F* adaptors employ negative pressure inside the vacuum chamber to form on demand a tight seal around the fluidic conduit. Subsequently, the embedded micro-tubes are attached to a syringe on a programmable syringe pump (PHD 2000, Harvard Apparatus) from which diluted aqueous-based color dye (Waterman, France) is perfused at various flow rates. All outflows are passively directed

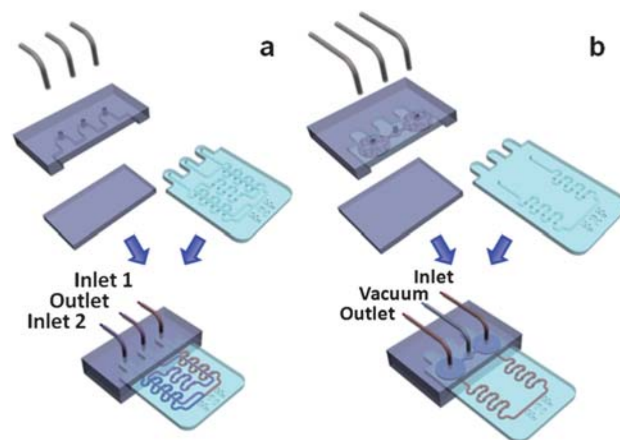

Fig. 3 Schematic illustration of the assembly process of a) *press-F2F* and b) *vacuum-F2F* connections.

to individual external reservoirs. Fig. 4 shows the experimental setup to assess the leakage pressure under a continuous fluidic flow. The relationship between the fluidic pressure and flow rate is determined by a calibration step using a pressure transducer (PX26 series, Omega) prior to the leakage test. For each characterization scheme, 8–10 devices have been fabricated and evaluated at a minimum of 3 trials each.

Plug-in alignment

Misalignment of both *press-F2F* and *vacuum-F2F* with pluggable microchips are optically measured using a digital camera (EC3, Leica) and a microscope (BH2-UMA, Olympus). Distinct alignment markers are placed on both the surface of the microchip and the flat inner socket surface such that through repeated plugging processes, displacements of these indicators are assessed.

Results and discussion

Adapting a similar concept to universal serial bus in microelectronics, the F2F Interconnects can serve as a standardized yet configurable interface to establish reliable and reversible connectivity between macro and micro components. Performances of the two unique F2F schemes, *press-F2F* and *vacuum-F2F* which do not rely on any chemical bond, but primarily on physical principles (either mechanical deformation or negative pressure), are thoroughly evaluated. Characteristic features of high-density tube packing and self-aligned plug-in are also discussed in detail in the following section. The proposed F2F techniques offer the world-to-chip interface novel universal configurations, which can be applied to a wide variety of lab-on-a-chip platforms.

Characterization of press-F2F scheme

(a) Leakage pressure *vs.* mechanical strain. *Press-F2F* connectors, operated under induced tensile stress, have been experimentally evaluated at the mechanical strain (ε) levels of 0.0%, 3.4%, 10.3%, 17.2%, and 24.1% ($\Delta h/h$, the ratio of the height difference between the plug-in and the socket to that of the socket). As mentioned earlier, the controlled strain is achieved by adjusting the thickness of the dry-film pluggable microchips. Fig. 5a shows the experimental measurements of the leakage pressure *versus* the theoretical predictions. As expected, an increasing trend of the leakage pressure is observed with the rising strain ultimately reaching the maximum leakage pressure of 58.6 kPa (±10.5 kPa) at 24% strain level. However, deviating from the theoretic calculation, measured leakage pressure shows improved performance in comparison with the prediction at lower strain levels (of 0.0% and 3.4%) because of interfacial adhesion between PDMS and dry-film surfaces.[35,36] Conversely, at higher strain levels (of 10.3%, 17.2%, and 24.1%), the experimental data become significantly less dependent on the induced strain, which is potentially attributable to out-of-plane bending as will be discussed in the following section. Subsequent increment in the strain level could cause severe resistance during the plug-in step and undesired mechanical stretch of the socket. Considering the non-leaking performance and easiness of plug-and-play operation, we conclude that the 10.3% strain level offers the optimal parameter for the *press-F2F* configuration.

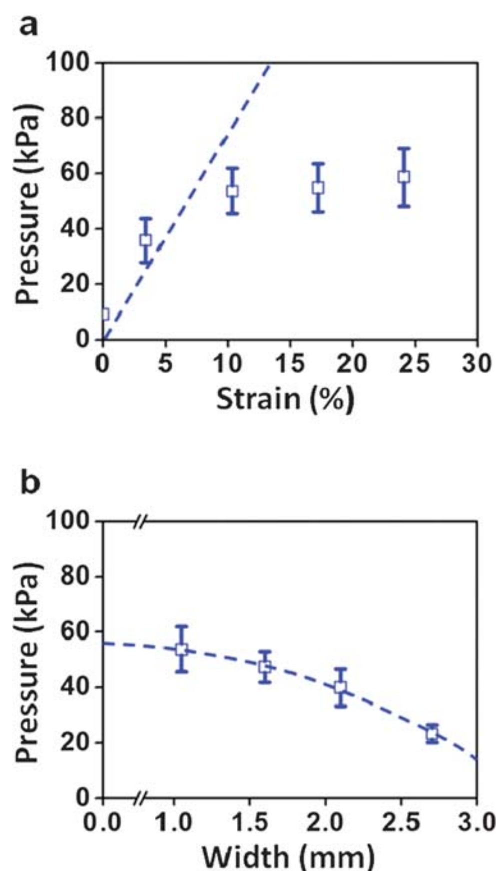

Fig. 5 Characterization of leakage pressure *vs.* a) tensile strain and b) structural width in the *press-F2F* configuration, respectively.

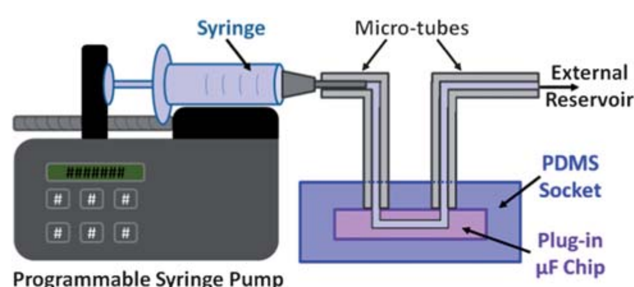

Fig. 4 Schematic illustration of the leakage test setup.

(b) Leakage pressure *vs.* structural width. Influence of the out-of-plan bending on the leakage pressure is further investigated through a series of controlled experiments conducted using peg-like structures with structural widths of 1.1, 1.6, 2.1, and 2.7 mm. Under the optimal strain level of 10.3% as aforementioned, the fluidic pressure acting on the center of the insertion area physically separates the PDMS socket from the dry-film microchip through mechanical bending in accordance with classical bending theory.[37] Theoretically, the threshold separation pressure is inversely proportional to the 2nd power of the structural width. The experimental results in Fig. 5b reflect such decreasing

 This journal is © The Royal Society of Chemistry 2010

trend with an approximated quadratic relation between the leakage pressure and the characteristic length (*i.e.*, the structural width). Leakage pressure drops drastically from 53.7 kPa (±8.1 kPa) to 23.3 kPa (±3.17 kPa) as increment of the structural width under the influence of the structural bending goes from 1.1 mm to 2.7 mm. However, further miniaturizing the dimension of the peg-like structures can cause difficulties in plug-in operation as well as reduced device reliability.

Characterization of vacuum-F2F scheme

Vacuum-F2F adaptors, sealed by the pressure difference between inside and outside of the vacuum chambers, have been fully characterized at various vacuum-to-fluid area ratios (*i.e.*, A_{vac}/A_{fluid} ratios of 0.7, 2.0, 3.3, and 4.7). As plotted in Fig. 6, the data points are acquired by supplying the negative pressure either through a facility vacuum line or a manual vacuum setup. As expected, the vacuum-seal strategy enables excellent on demand non-leaking performance following a linear relationship between the leakage pressure and the vacuum-to-fluid area ratio. By using the facility vacuum line (at a negative pressure of 85 kPa), the maximal leakage pressure is measured as high as 336.1 kPa (±2.5 kPa) under the area ratios of 4.7, which is substantially more powerful and more consistent (*i.e.*, narrower standard deviations) than the press-fit counterpart, although bounded to the vacuum access. Further increase in the A_{vac}/A_{fluid} ratio can lead to higher packaging performance as previously noted in the Concept section. In the case where access to the vacuum line is restricted, a proposed manual vacuum generation method utilizing a spring-loaded syringe can provide a negative pressure averaging 47.9 kPa, as shown in Fig. S1 (see ESI†). Similarly, the maximum performance of 197.4 kPa (±6.6 kPa) is measured at the vacuum-to-fluid area ratio of 4.7.

In summary, the *vacuum-F2F* strategy comes with an easy-to-implement, on demand vacuum seal that is highly adaptive to cases where high pressure/high flow rates are necessary for reliable on-chip functionality. On the other hand, in the scenario where low flow rates apply, the *press-F2F* could be the better option due to its simplicity.

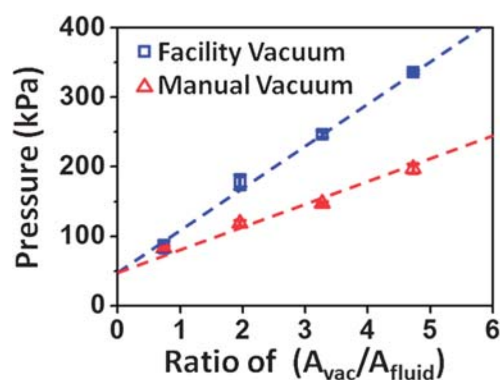

Fig. 6 Characterization of leakage pressure *vs.* ratio of vacuum-to-fluid area in *vacuum-F2F* settings. The vacuum pressures are provided by either the facility's vacuum line (in blue) or a spring-loaded syringe (in red).

Two-dimensional micro-tube packing

High micro-tube packing density of 1 tube/mm^2 in two-dimensional array arrangement is applicable to both *press-F2F and vacuum-F2F* configurations. Here, the center-to-center distance of access ports can be reliably placed within 1 mm of each other without spatial obstructions. For *vacuum-F2F* adaptors, the locations of micro-tube insertions are conveniently designated by the assisting o-ring seats. In Fig. 7, a 6-level chemical gradient generator has been devised to demonstrate the 2D configurability *via* a 3-by-3 access port array (with 18 mm^2 overall area) in which two are dedicated for injection, six for individual chemical drain, and the last one for vacuum seal. To our best knowledge, the F2F Interconnects enable the highest density of tube-packing in a unique 2D configuration and offers easy configurability and expandability, which is of particular use for large-scale integrated and multitasking microfluidics.

Precision of self-aligned plug-in

In the F2F designs, alignment of the microfluidic chip to the PDMS socket is ensured by the simple peg-in-hole principle. The on-chip peg-like structures (1 mm in width) serve as guides to enhance accurate fitting to the complementary shapes in the elastomeric adaptor during the manual insertions. Average misalignment of the self-guided peg-like structures is 10.7 μm (±9.9 μm). This simple plug-in methodology using only complementary peg-like structures allows F2F Interconnects to have the capability of granting highly reliable connectivity. In addition, the reusability of both F2F Interconnect configurations have been tested more than 100 times, from which no appreciable degradation in the sealing or plug-in performance has been noticed.

Conclusions

In this paper, we have developed standardized macro-to-microfluidic adaptors, referred to as Fit-to-Flow (F2F) Interconnects that operate through either press-fit or vacuum-seal

Fig. 7 Photography of a 6-level chemical gradient generator plugged into a vacuum-F2F adaptor with a 3 × 3 array of access ports in side-by-side comparison to a USB flash drive with UC Davis logo.

configurations, to provide truly reversible attachments and connections between peripheral setups and microfluidic devices. In particular, the F2F technology includes an array of highly favorable features for emerging biofluidic operations, including (a) outstanding non-leaking performance (up to 336 kPa), (b) high-density 2D tube-packing (1 tube/mm^2), (c) self-guided alignment, (d) reworkable connectivity or device reusability, (e) general applicability to regular lab settings, (f) simple processing, as well as (g) microfabrication-compatibility allowing the connections to be easily expanded, miniaturized, and reconfigured. Applicability of F2F technology to common microfluidic operations has been well demonstrated in 3D chaotic mixing and 6-level chemical gradient generator. Potential implementations of the novel F2F Interconnects can be universally extended to lab-on-a-chip systems involving point-of-care diagnosis, cellular sensing and manipulation, and controlled drug delivery.

Acknowledgements

This work is in part supported by the National Science Foundation CAREER Program (ECCS-0846502). AC would like to acknowlege the fellowship support from the University of California, Davis. Authors also acknowledge DuPont Company for generously providing PerMX dry-film samples.

References

1 A. M. Skelley, O. Kirak, H. Suh, R. Jaenisch and J. Voldman, *Nat. Methods*, 2009, **6**, 147–152.
2 A. L. Paguirigan and D. J. Beebe, *BioEssays*, 2008, **30**, 811–821.
3 H. Yu, C. M. Alexander and D. J. Beebe, *Lab Chip*, 2007, **7**, 388–391.
4 K. Ohno, K. Tachikawa and A. Manz, *Electrophoresis*, 2008, **29**, 4443–4453.
5 S. Kim, B. Huang and R. N. Zare, *Lab Chip*, 2007, **7**, 1663–1665.
6 E. Delamarche, A. Bernard, H. Schmid, B. Michel and H. Biebuyck, *Science*, 1997, **276**, 779–781.
7 C. Zhang, K. Khoshmanesh, A. Mitchell and K. Kalantar-zadeh, *Anal. Bioanal. Chem.*, 2010, **396**, 401–420.
8 J. J. Agresti, E. Antipov, A. R. Abate, K. Ahn, A. C. Rowat, J. C. Baret, M. Marquez, A. M. Klibanov, A. D. Griffiths and D. A. Weitz, *Proc. Natl. Acad. Sci. U. S. A.*, 2010, **107**, 4004–4009.
9 S. Y. Teh, R. Lin, L. H. Hung and A. P. Lee, *Lab Chip*, 2008, **8**, 198–220.
10 T. P. Hunt, D. Issadore and R. M. Westervelt, *Lab Chip*, 2008, **8**, 81–87.
11 N. Pamme, *Lab Chip*, 2007, **7**, 1644–1659.
12 G. M. Whitesides, *Nature*, 2006, **442**, 368–373.
13 D. J. Beebe, G. A. Mensing and G. M. Walker, *Annu. Rev. Biomed. Eng.*, 2002, **4**, 261–286.
14 A. Arora, G. Simone, G. B. Salieb-Beugelaar, J. T. Kim and A. Manz, *Anal. Chem.*, 2010, **82**, 4830–4847.
15 M. Zhang, J. Wu, L. Wang, K. Xiao and W. Wen, *Lab Chip*, 2010, **10**, 1199–1203.
16 L. Tang and N. Y. Lee, *Lab Chip*, 2010, **10**, 1274–1280.
17 M. Quaglio, G. Canavese, E. Giuri, S. L. Marasso, D. Perrone, M. Cocuzza and C. F. Pirri, *J. Micromech. Microeng.*, 2008, **18**, 055012.
18 J. S. Kuo, Y. Zhao, L. Ng, G. S. Yen, R. M. Lorenz, D. S. Lim and D. T. Chiu, *Lab Chip*, 2009, **9**, 1951–1956.
19 K. Aran, L. A. Sasso, N. Kamdar and J. D. Zahn, *Lab Chip*, 2010, **10**, 548–552.
20 S. G. Im, K. W. Bong, C. H. Lee, P. S. Doyle and K. K. Gleason, *Lab Chip*, 2009, **9**, 411–416.
21 C. H. Chiou and G. B. Lee, *J. Micromech. Microeng.*, 2004, **14**, 1484–1490.
22 J. de Jong, R. G. Lammertink and M. Wessling, *Lab Chip*, 2006, **6**, 1125–1139.
23 H. Wu, B. Huang and R. N. Zare, *Lab Chip*, 2005, **5**, 1393–1398.
24 V. Saarela, S. Franssila, S. Tuomikoski, S. Marttila, P. Östman, T. Sikanen, T. Kotiaho and R. Kostiainen, *Sens. Actuators, B*, 2006, **114**, 552–557.
25 A. M. Christensen, D. A. Chang-Yen and B. K. Gale, *J. Micromech. Microeng.*, 2005, **15**, 928–934.
26 A. A. S. Bhagat, P. Jothimuthu, A. Pais and I. Papautsky, *J. Micromech. Microeng.*, 2007, **17**, 42–49.
27 E. Tkachenko, E. Gutierrez, M. H. Ginsberg and A. Groisman, *Lab Chip*, 2009, **9**, 1085–1095.
28 U. Y. Schaff, M. M. Xing, K. K. Lin, N. Pan, N. L. Jeon and S. I. Simon, *Lab Chip*, 2007, **7**, 448–456.
29 D. Sabourin, D. Snakenborg and M. Dufva, *J. Micromech. Microeng.*, 2009, **19**, 035021.
30 J. Melin and S. R. Quake, *Annu. Rev. Biophys. Biomol. Struct.*, 2007, **36**, 213–231.
31 T. Thorsen, S. J. Maerkl and S. R. Quake, *Science*, 2002, **298**, 580–584.
32 S. Zhao, H. Cong and T. Pan, *Lab Chip*, 2009, **9**, 1128–1132.
33 D. Anderson and D. Dzatko, *Universal Serial Bus System Architecture*, Addison-Wesley, 2001.
34 F. Beer, E. R. Johnston, J. DeWolf and M.D., *Mechanics of Materials*, McGraw-Hill, 2008.
35 K. J. Hsia, Y. Huang, E. Menard, J. U. Park, W. Zhou, J. Rogers and J. M. Fulton, *Appl. Phys. Lett.*, 2005, **86**, 154106.
36 M. K. Chaudhury and G. M. Whitesides, *Langmuir*, 1991, **7**, 1013–1025.
37 W. C. Young and R. G. Budynas, *Roark's Formulas for Stress and Strain*, McGraw-Hill, 2002.

 This journal is © The Royal Society of Chemistry 2010